Design of Mach-Zehnder modulators and contra-directional couplers.

BENJAMIN CROCKETT (EDX USERNAME: BENCROCK, GITHUB: BAYSEE)[1*]

[1]*Institut national de la recherche scientifique—Centre Énergie Matériaux Communications, Montréal, Québec H5A 1K6, Canada*
**Benjamin.crockett@inrs.ca*

Abstract: In this report, we review the basic design flow for general integrated silicon photonics components. We first review the physics of waveguide propagations, and how they can be modelled using an eigenmode solver via Matlab. We then use basic building blocks developed within the SiEPIC program which have been characterized through both simulation and experimental experiments. In particular, we build Mach Zehnder interferometers (MZI) and contra-directional couplers (CDC), from which we retrieve the basic circuit parameters through analytical derivations and simulations.

[fork link: https://github.com/Baysee/openEBL-2025-02/tree/main/submissions]

1. Introduction

In this report, we review the basic implementation of silicon waveguides for TE polarization. We then design a set of Mach-Zehnder interferometers from which we can retrieve the group index of the waveguide. Finally, we include basic information about the implementation of contra-directional couplers. These designs are still in progress, as issues with connecting KLayout to Lumerical Mode were encountered which halted the progress of these components.

2. Waveguide geometry and index

The waveguide has the usual dimensions for TE polarization, namely a width of 500 nm and a height of 220 nm. Note that the index of refraction n is a property of a material itself, which describes how much the optical wave is slowed down compared to propagation in vacuum (i.e., the phase velocity of the wave in a given medium), assuming a large enough bulk material such that its geometry has no impact on the wave propagation. On the other hand, effective index of refraction n_{eff} captures how the wave propagates by including not only the material property, but also the waveguide geometry, which becomes significantly different from the regular index of refraction when the mode area is on a similar order of size as the waveguide geometry.

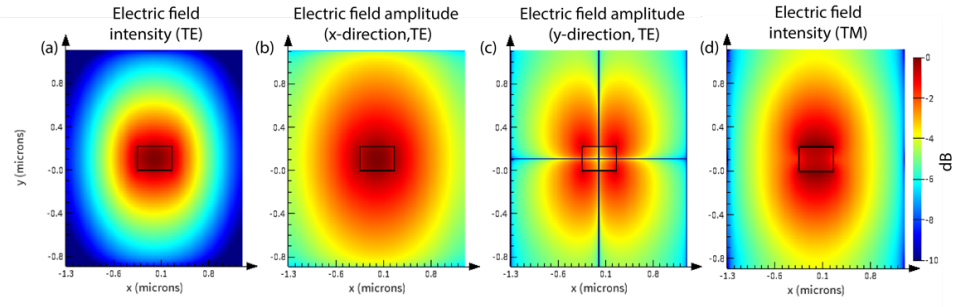

Fig. 1. Simulated waveguide mode profile. The waveguide dimensions are shown by the rectangle at the center of each figure. (a) The electric field intensity. We confirm that the simulation bounds are properly set since the intensity falls to a relative value of ~-10 dB when compare to the maximum value. (b) Electric field amplitude in the x-direction, and (c) in the y-direction. (d) Electric field intensity of the first TM mode. Observe that the intensity in mainly confined outside of the waveguide. These simulations confirm our waveguide carries TE polarization, where the main electric field component is parallel to the wafer (x-direction). Note that the color bar applies to all plots.

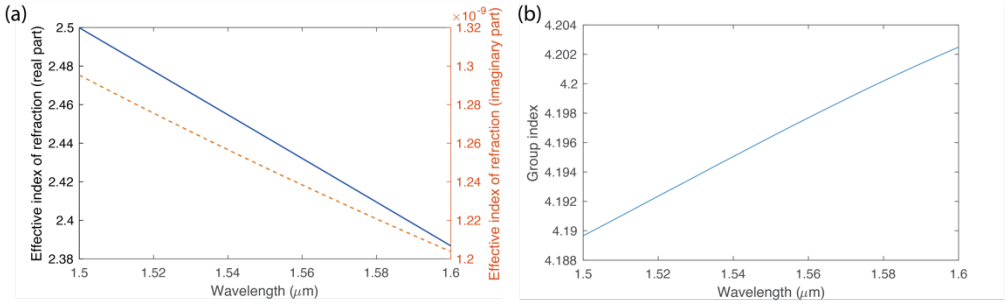

Fig. 2. Wavelength dependence of (a) the real part (blue trace, left axis) and imaginary part (orange dashed trace, right axis) of the index of refraction, and (b) wavelength dependence of the group index.

The mode profiles for the silicon waveguide described above is shown in Fig. 1. In Fig. 1(a), we plot the electric field intensity. Notice that the intensity drops significantly on the outer edges, confirming that we chose the right size for the simulation area. The x-component of the electric field is shown in Fig. 1(b), which is much more significant than the y-component shown in Fig. 1(c), confirming that we have a TE polarization. Notice the low amplitude regions along the center in Fig. 1(c). This is hypothesized to be a numerical artifact. Finally, we also plot the electric field intensity of the first TM mode, which can be seen to be mainly confined outside of the waveguide, as expected. The resulting effective index of refraction is plotted in Fig. 2, with a real value of ~2.43 near 1550 nm. The imaginary part, representing absorbtion, is significantly smaller, on the order of 1×10^{-9}.

On the other hand, the group index n_g describes the group velocity of a wave, which describes namely the speed at which a pulse of a certain wavelength would propagate. It can be expressed in terms of the effective index as

$$n_g = n_{\text{eff}} - \lambda \frac{dn_{\text{eff}}}{d\lambda}. \tag{1}$$

The compact model for the waveguide is $n_{\text{eff}}(\lambda) = n_1 + n_2(\lambda - \lambda_0) + n_3(\lambda - \lambda_0)^2$, where the coefficients are found to be $n_1 = 2.44$, $n_2 = -1.13$, and $n_3 = -0.041$ by fitting the curve shown in Fig. 2(b).

3. Circuit geometry and functionality

Three MZI configurations were tested, shown in Table 1, as well as 5 CDC configurations, shown in Table 2.

3.1 Imbalanced Mach-Zehnder interferometer

UAs a first circuit, we consider an imbalanced interferometer with a Mach-Zehnder interferometer. This circuit is characterized by a path length difference ΔL. The interference caused by the two paths recombining depends on waveguide's propagation constant $\beta = \frac{2\pi n}{\lambda}$, where n is the index of refraction of the waveguide and λ the optical wavelength, and on ΔL as

$$\frac{I_0}{I_i} = \frac{1}{2}[1 + \cos(\beta \Delta L)]. \tag{2}$$

An important metric for this circuit is the free spectral range (FSR) which characterizes the period of the oscillations in the spectral domain. It can be found with eq. (2) by solving for $FSR = \lambda_{m+1} - \lambda_m$, where λ_m is the wavelength of the m^{th} peak, which occur for a phase difference of 2π in the argument of the cosine. In particular, we find that there must be a

difference of $\Delta\beta = \frac{2\pi}{\Delta L}$ between the propagation constant of each peaks, which we approximate to vary linearly with λ

$$\Delta\beta \approx -\frac{d\beta}{d\lambda}\Delta\lambda. \quad (3)$$

Since $\beta = \frac{2\pi n}{\lambda}$, we can rewrite its wavelength dependence as

$$\frac{d\beta}{d\lambda} = \frac{2\pi}{\lambda}\frac{dn}{d\lambda} - \frac{2\pi n}{\lambda^2} = -\frac{2\pi}{\lambda^2}n_g, \quad (4)$$

Table 1: Circuit parameters

Device name	Properties	Notes
Marker 1	L: 162.9 um 2x5 um bends	
MZI 1	L_1: 149.377 L_2: 612.06 ΔL: 462.683	Theoretical FSR: 1.24 nm Simulated FSR: 1.24 nm Measured FSR: 1.252 nm ($n_g = 4.161$)
MZI2	L_1: 149.377 L_2: 379.031 ΔL: 229.65	Theoretical FSR: 2.49 nm Simulated FSR: 2.49 nm Measured FSR: 2.523 nm ($n_g = 4.183$)
MZI3	L_1: 149.377 L_2: 233.130. ΔL: 83.75	Theoretical FSR: 6.84 nm Simulated FSR: 6.83 nm Measured FSR: 6.899 nm ($n_g = 4.183$)

Where we used the definition of the group index shown in Eq. (1). Now that we have an explicit expression for the wavelength dependence of the propagation constant in terms of measurable variables, we can insert it into eq. (3) and solve for $\Delta\lambda$, finding that the FSR depends on the waveguide and optical properties as $\text{FSR} = \frac{\lambda^2}{\Delta L\, n_g}$.

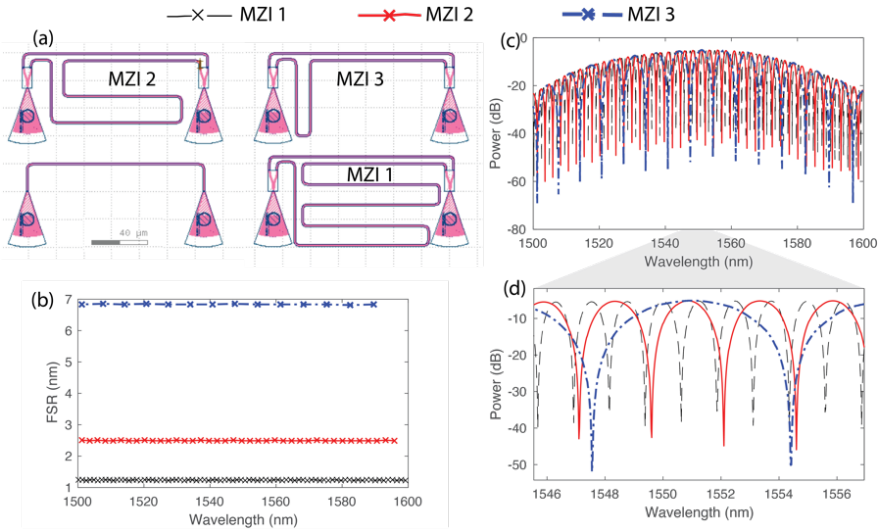

Fig. 3. Interferometer design and simulation. (a) screen shot of the GDS file. (b) FSR values for the different designs. (c) Spectral response, showing the response of the grating coupler over a broad range, and (d) a zoomed-in version, showing the variation of the FSR.

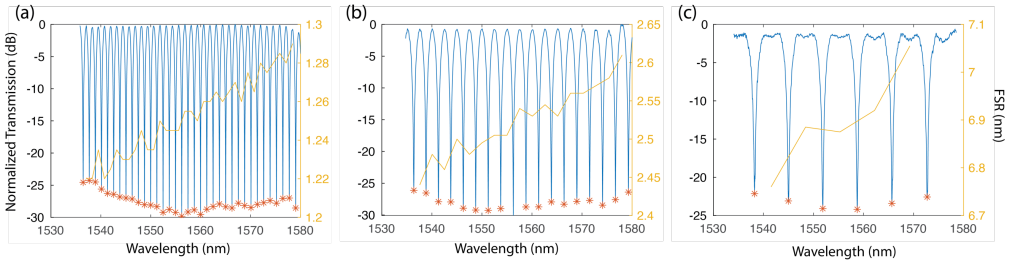

Fig. 4. Interferometer experimental results, showing on the left axis the transmitted light in blue and the identified dips with the orange asterisks, and on the right axis the FSR in yellow. (a) MZI1 (b) MZI2 (c) MZI3.

A schematic of the interferometers is shown in Fig. 3(a), which also depicts an alignment marker which will be use to de-embed the impact of the grating couplers. The simulated FSRs are shown in Fig. 3(b), yielding mean FSRs of 1.24, 2.49 and 6.83 nm for MZI 1, 2 and 3, respectively. The extracted measurement results, where the response of the grating couplers have been compensated, are shown in Fig. 4. The simulation and experimental values are in agreement with the analytically predicted ones shown in Table 1.

3.2 Contra-directional couplers

Contra-directional couplers (CDC) broadly correspond to a photonic circuit composed of two closely spaced waveguide, where the coupling region is designed such that light of a given wavelength at the input will reflect and couple to the adjacent waveguide, out of the drop port, while the rest of the frequency components propagate out of the through port [2]. One possible implementation is by having both waveguides as Bragg waveguides geometry as shown in Fig. 5 (a), where both waveguides also have different widths W and corrugation widths ΔW repeating with a period Λ (for N periods, resulting in a total length $L = N\Lambda$). These different waveguide geometries lead to different effective index of refraction $n_{in,d}$ and propagation constants $\beta_{in,d}$. Thus, this implements a notch filtering centered at a wavelength $\lambda_d = 2n_{av}\Lambda$, (at ~1546 nm in Fig. 5(a)), where $n_{av} = (n_{in} + n_d)/2$. Note that there may be backscattering within each waveguide (i.e., not coupling from one waveguide to the other) at the Bragg wavelengths $\lambda_{in} = 2n_{in}\Lambda$ and $\lambda_d = 2n_d\Lambda$; this is typically undesired, and ultimately limits the usable bandwidth of the CDC [3]. The design employed here uses an out-of-phase grating to suppress these back reflections [3], as well as gaussian apodization to slowly increase the coupling coefficient κ thereby avoiding a steep change of the index [4].

The coupling coefficient κ is a function of the electric field mode profiles $E_{in}(x, y)$ and $E_d(x, y)$, as well as the dielectric disturbance $\Delta\epsilon_p(x, y)$, for transverse coordinates x and y. This dielectric disturbance function describes the 2D distribution of the disturbance (waveguide widths, gap, corrugation, etc.), while the entire waveguide can be described in 3D via $\Delta\epsilon(x, y, z) = S(z)\epsilon_p(x, y)$, where $S(z)$ is a periodic function (ignoring apodization, for simplicity). Specifically, κ can be derived using coupled mode theory as [2]

$$\kappa = \frac{\pi c S_1}{2\lambda_d} \iint E_a^*(x, y)\Delta\epsilon(x, y)E_b(x, y)dxdy$$

Where S_1 is the first-order Fourier expansion coefficient of $S(z)$. From this factor, we can then calculate the reflectivity (amount of light transferred to the adjacent waveguide) as

$$\eta = \frac{|\kappa|^2 \sinh(sL)}{s^2 \cosh(sL) + \Delta\beta^2/4 \sinh(sL)}$$

Where $\Delta\beta = \beta_a^+ - \beta_b^- - 2\pi\Lambda$ and $s^2 = |\kappa|^2 - \Delta\beta^2/4$. The range of wavelengths over which this reflectivity is significant dictates the bandwidth of the notch, which can be expressed as

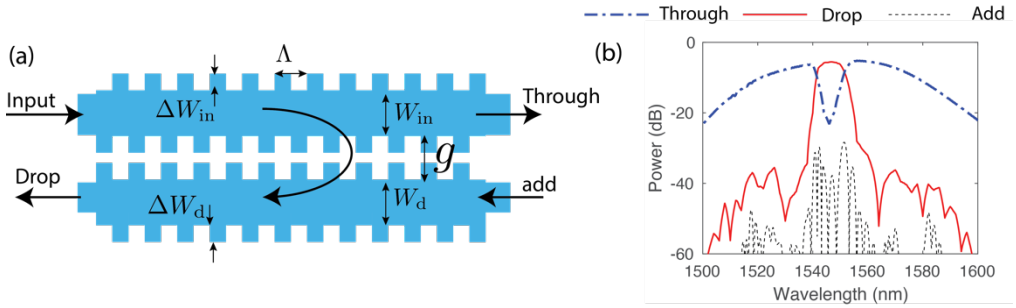

Fig. 5. (a) depiction of a contra directional coupler. W_{in} and W_{d} are the widths of the input and drop waveguide, respectively, with corresponding corrugation widths ΔW_{in} and ΔW_{d}. Λ is the grating period and g is the gap width. are the corrugation widths of the Input corre (b) results of the simulation for CDC1.

$$\Delta\lambda = \frac{2\lambda^2\kappa_0}{\pi(n_1 + n_2)}$$

where we approximate that the effective refractive indices are constant over wavelength and that we are in the strong coupling regime [5]. It has been shown that the bandwidth decreases with increasing gap g and decreasing corrugation width [6,7].

In this study, we wish the study in the impact of the corrugation and gap widths on the bandwidth. As a baseline, we take the default parameters from the default CDC in the SiEPIC package, shown in Table 2, which leads to the simulation shown in Fig. 5 (b). Two variations on the corrugation widths are made, to have widths of 40 nm and 15 nm for the input and drop waveguides, and 60 nm and 25 nm for the same waveguides. This is done while keeping the gap constant at 100 nm. For the two additional devices, we keep the corrugation widths the same, but have the gaps as 80 nm and 120 nm.

The experimental results are shown in Fig. 6. Unfortunately, CDC1 (with the default design parameters) and CDC 2 did not return any meaningful transmission on any of the ports. CDC3 returned an asymmetric response between the add and drop port, CDC4 has a strange response where the drop and through port seem somehow inverted, and CDC5 has a relatively normal reponse. The details of the different widths are shown in Table 2.

Comparing the simulation of CDC1 vs the results of CDC3, the gap were the same but the corrugation width was smaller for CDC3. We would therefore expect a smaller bandwidth, which is the case for the through port, but not the drop port. Comparing CDC1 and CDC5, the corrugation width was the same but the gap was larger for CDC3, so we would expect a lower bandwidth. However this was not the case. Therefore, a better understanding of fabrication imperfections would be needed moving forward.

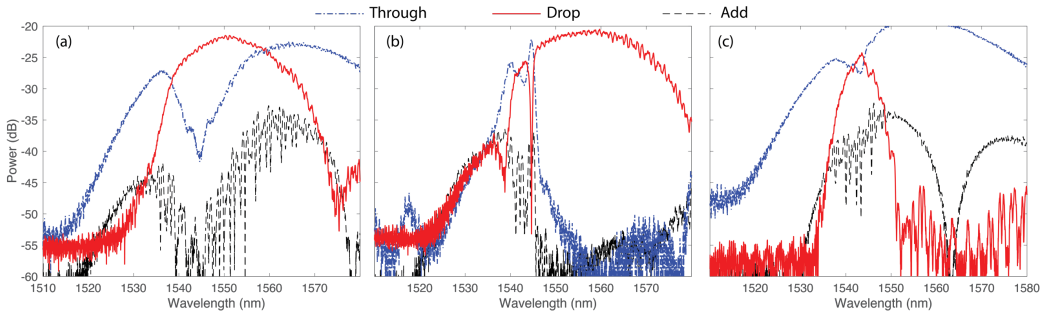

Fig. 6. Experimental results for (a) CDC3, (b) CDC4, and (c) CDC 5.

Table 2: CDC circuit parameters

Device name	Properties	Notes
CDC1	Spacing: 0.316 Number of grating periods: 1000 WG1 width: 560 nm WG2 width: 440 nm ΔW_{in} corrugation width: 50 nm ΔW_{d} corrugation width: 25 nm Gap width: 100 nm	Default design parameters Simulation results: Through 3-dB bandwidth: 3.53 nm Drop 3-dB bandwidth: 9.92 nm Experiment did not work.
CDC2	ΔW_{in} corrugation width: 40 nm ΔW_{d} corrugation width: 15 nm Gap width: 100 nm	Experiment did not work.
CDC3	ΔW_{in} corrugation width: 60 nm ΔW_{d} corrugation width: 35 nm Gap width: 100 nm	Through 3-dB width: 1.74 nm Through 10-dB width: 10.3 nm Drop 3-dB width: 17.9 nm Drop 10-DB width: 31.0 nm
CDC4	ΔW_{in} corrugation width: 50 nm ΔW_{d} corrugation width: 25 nm Gap width: 80 nm	Drop and add port seem inverted, with a very narrow response. Only the 3-dB width is given due to the weird shape. Through 3-dB width: 1.08 Drop 3-dB width: <0.04 nm
CDC5	ΔW_{in} corrugation width: 50 nm ΔW_{d} corrugation width: 25 nm Gap width: 120 nm	Through port shows a very shallow dip, so only the 2-dB width is given. The response is relatively symmetrical between both ports. Through 2-dB width: 4.94 nm Drop 2-dB width: 2.5 nm

4. Conclusion

In conclusion, we reviewed the design of Mach-Zehnder interferometer and contra-dictional couplers on silicon. For the interferometer, we predicted the FSR for different path imbalances, both through analytical derivations and simulations. For the contradirectional couplers, we reviewed the basic theory and proposed designs to study the effect of corrugation and gap width

on the bandwidth. Further simulations and experiments are needed to better understand the behaviour of the CDC.

References

1. R. Boeck, M. Caverley, L. Chrostowski, and N. A. F. Jaeger, "Process calibration method for designing silicon-on-insulator contra-directional grating couplers," Opt. Express **23**, 10573 (2015).
2. P. Yeh and H. F. Taylor, "Contradirectional frequency-selective couplers for guided-wave optics," Appl. Opt. **19**, 2848 (1980).
3. W. Shi, H. Yun, C. Lin, M. Greenberg, X. Wang, Y. Wang, S. T. Fard, J. Flueckiger, N. A. F. Jaeger, and L. Chrostowski, "Ultra-compact, flat-top demultiplexer using anti-reflection contra-directional couplers for CWDM networks on silicon," Opt. Express **21**, 6733 (2013).
4. J. Cauchon, "Thesis: Silicon Photonic Bragg-Based Devices : Hardware and Software," (2021).
5. D. Marcuse, "Bandwidth of forward and backward coupling directional couplers," J. Lightwave Technol. **5**, 1773–1777 (1987).
6. W. Shi, X. Wang, W. Zhang, L. Chrostowski, and N. A. F. Jaeger, "Contradirectional couplers in silicon-on-insulator rib waveguides," Opt. Lett. **36**, 3999 (2011).
7. K. Ikeda, M. Nezhad, and Y. Fainman, "Wavelength selective coupler with vertical gratings on silicon chip," Applied Physics Letters **92**, 201111 (2008).